Seventh International Conference on CFD in the Minerals and Process Industries
CSIRO, Melbourne, Australia
9-11 December 2009

CFD MODELLING OF ARC WELDING – THE IMPORTANCE OF THE ARC PLASMA

Anthony B. MURPHY[1], Manabu TANAKA[2], Kentaro YAMAMOTO[2], Shinichi TASHIRO[2] and John J. LOWKE[1]

[1] CSIRO Materials Science and Engineering, PO Box 218, Lindfield NSW 2070, AUSTRALIA
[2] Joining and Welding Research Institute, Osaka University, 11-1 Mihogaoka, Ibaraki, Osaka 567-0047, JAPAN

ABSTRACT

We have applied computational fluid dynamic modelling techniques to the simulation of arc welding. A feature of our work is that the electrode, arc plasma and workpiece are all included in the computational domain, and are treated self-consistently. We demonstrate the importance of including the arc plasma in the computational domain with three examples. First, we have examined the influence of the shielding gas composition on the arc and weld pool properties, and have related this to the thermophysical properties of the gas. This research has allowed improved shielding gases and welding processes to be developed. In a second example, the vaporisation of the weld pool metal, and the diffusion of the vapour into the arc plasma, have been simulated. The effect of the metal vapour can be very significant. It cools the plasma through increased radiative emission, and decreases the current density to the workpiece through increased electrical conductivity at lower temperatures. These effects in turn strongly influence the weld pool properties. Finally, we have investigated the influence of the electrode shape. Again we find that the effect on the arc parameters, and consequently the weld pool, is substantial.

NOMENCLATURE

$\mathbf{A}$	magnetic potential
$\mathbf{B}$	magnetic field strength
c_p	specific heat at constant pressure
e	electronic charge
$\mathbf{g}$	gravitational acceleration
h	specific enthalpy
$\mathbf{j}$	current density
j_e	electron current density
$\mathbf{J}_M$	diffusion mass flux of metal species
k	thermal conductivity
k_B	Boltzmann's constant
P	pressure
P_a	pressure on arc side of arc–workpiece interface
P_w	pressure on workpiece side of interface
r	radial coordinate
t	time
T	temperature
U	net radiative emission coefficient
$\mathbf{v}$	velocity
V_i	ionisation energy of shielding gas
x_i	coordinates in three-dimensional geometry
$x_\square$	displacement parallel to arc–workpiece interface
Y_M	mass fraction of metal species
z	axial coordinate
ϕ	electric potential
φ_w	work function of workpiece material
γ	surface tension of weld pool
η	dynamic viscosity
κ	surface curvature of weld pool
μ_0	permittivity of free space
ρ	mass density
σ	electrical conductivity
$\underset{\sim}{\boldsymbol{\tau}}$	stress tensor
τ_a	shear stress on arc side of arc–workpiece interface
τ_w	shear stress on workpiece side of interface

INTRODUCTION

Probably the predominant aim of computational simulations of arc welding is to understand and if possible predict properties of the weld. Consequently, most simulations focus on phenomena in the workpiece, including the molten weld pool, with the arc plasma only included through boundary conditions, such as the heat flux distribution and arc pressure at the workpiece surface.

We present three examples that demonstrate that accurate predictions of the weld pool properties are not possible if the arc plasma is not explicitly included in the computational domain. We use a model in which the electrodes and arc are included self-consistently. We examine (1) the influence of shielding gas composition in tungsten–inert-gas (TIG) welding; (2) the influence of metal vapour emanating from the weld pool in TIG welding; and (3) the effect of the wire electrode shape in MIG (metal–inert-gas) welding. We show that the properties of the arc that influence the weld pool depth and geometry are strongly affected by the shielding gas composition, metal vapour, and the electrode shape.

MODEL DESCRIPTION

Four conservation equations are solved. The equation of conservation of mass is:

$$\frac{\partial \rho}{\partial t} + \nabla \cdot (\rho \mathbf{v}) = 0. \qquad (1)$$

The equation of momentum conservation is:

$$\frac{\partial (\rho \mathbf{v})}{\partial t} + \nabla \cdot (\rho \mathbf{v}\mathbf{v}) = -\nabla P - \nabla \cdot \underset{\sim}{\boldsymbol{\tau}} + \mathbf{j} \times \mathbf{B} + \rho \mathbf{g}. \qquad (2)$$

The terms on the right-hand side describe respectively the forces due to pressure gradients, viscous stress, the

Lorentz or magnetic pinch force, and gravity. The stress tensor is given in Cartesian geometry by

$$\tau_{ii} = \eta\left(2\frac{\partial v_i}{\partial x_i} - \frac{2}{3}\nabla\cdot\mathbf{v}\right),$$
$$\tau_{ij} = \eta\left(\frac{\partial v_i}{\partial x_j} + \frac{\partial v_j}{\partial x_i}\right), \quad i \neq j. \tag{3}$$

The equation of energy conservation is

$$\frac{\partial(\rho h)}{\partial t} + \nabla\cdot(\rho\mathbf{v}h) = \frac{\mathbf{j}^2}{\sigma} - U - \nabla\cdot\left(\frac{k}{c_p}\nabla h\right) + \frac{5k_B}{2ec_p}\mathbf{j}\cdot\nabla h. \tag{4}$$

The terms on the right-hand side describe respectively resistive heating, radiative emission, thermal conduction, and energy transfer arising from the flow of electrons. The enthalpy is the integral of specific heat with respect to temperature, and the temperature at any position is easily derived from the enthalpy at that position. Finally, the equation of current continuity is

$$\nabla\cdot\mathbf{j} = \nabla\cdot\left(\sigma\nabla\phi\right) = 0. \tag{5}$$

The magnetic field strength $\mathbf{B}$, which appears in equation (2), also has to be calculated. This can be done by solving for the magnetic potential $\mathbf{A}$:

$$\nabla^2\mathbf{A} = -\mu_0\mathbf{j}, \tag{6}$$

and using $\mathbf{B} = \nabla\times\mathbf{A}$. For axisymmetric geometry, it is usually a good approximation to use only the azimuthal component of the magnetic field strength

$$B_\theta(r) = \frac{\mu_0}{r}\int_0^r r' j_z\, dr'. \tag{7}$$

The TIG and MIG welding models use two-dimensional axisymmetric, and three-dimensional Cartesian geometry, respectively. Equations (1) to (5) are solved in the respective geometries, with the magnetic field obtained using Eqs. (7) and (6), respectively. The equations are solved using the finite volume method of Patankar (1980), incorporating the SIMPLEC algorithm of van Doormaal and Raithby (1984).

The computational domain for two-dimensional axisymmetric geometry is shown in Fig. 1. On the axis ($r = 0$), derivatives of all quantities with respect to radius are set to zero. The temperature at the external boundaries is set to 300 K. The axial velocity boundary condition at the upper boundary gf in Fig. 1 is used to define the input flow rate of the shielding gas. The derivatives of the velocity components are zero at the radial boundary fe. The pressure needs only to be defined at one point; it is set to 1 atm at point f. The axial current density at ag is chosen so that the integral over the cross-section at the top of the cathode is equal to the arc current. The electrical potential is set to 0 V at point d. The external boundary conditions for the three-dimensional Cartesian geometry are analogous, but there is no line of symmetry through the centre of the top electrode.

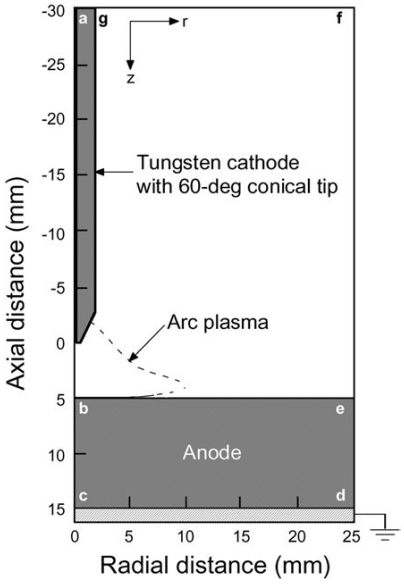

Figure 1: Computational domain for TIG welding, showing the external and internal boundaries. From Tanaka and Lowke (2007).

The boundary conditions at the internal boundaries between the electrodes and plasma have to be treated carefully. Four physical factors are important in determining the influence of the arc plasma on the weld pool: (a) the heat flux, (b) the current density, (c) the shear stress, and (d) the arc pressure, all at the weld pool surface. All four factors feature in the boundary conditions at the interface between the arc and the workpiece.

The heat flux to the workpiece is different for TIG and MIG welding, since the polarity is different. In MIG welding, the workpiece is a non-thermionic cathode, for which the electron emission mechanism is not well understood. In TIG welding, the workpiece is the anode. We use the following expressions for the heat flux (Tanaka and Lowke, 2007; Lowke and Tanaka, 2008):

$$S = j_e\varphi_w - k\,\partial T/\partial z \quad \text{(TIG welding)},$$
$$S = j_e\left(V_i - \varphi_w\right) - k\,\partial T/\partial z \quad \text{(MIG welding)}. \tag{8}$$

In each case, the first term describes heating due to electron flux, and the second due to thermal conduction. The boundary conditions for momentum transfer across the arc–weld-pool interface are

$$\tau_a - \tau_w + \left(d\gamma/dT\right)\left(dT/dx\right) = 0,$$
$$P_a - P_w + \gamma\kappa = 0, \tag{9}$$

parallel and perpendicular to the weld pool surface, respectively. The parallel boundary condition shows that the difference in shear stress across the interface is determined by the Marangoni term $d\gamma/dx$, which describes the variation of the surface tension due to the gradient of temperature close to the weld pool surface. The perpendicular boundary condition shows that the pressure difference across the interface is determined by the product of the surface tension and the curvature.

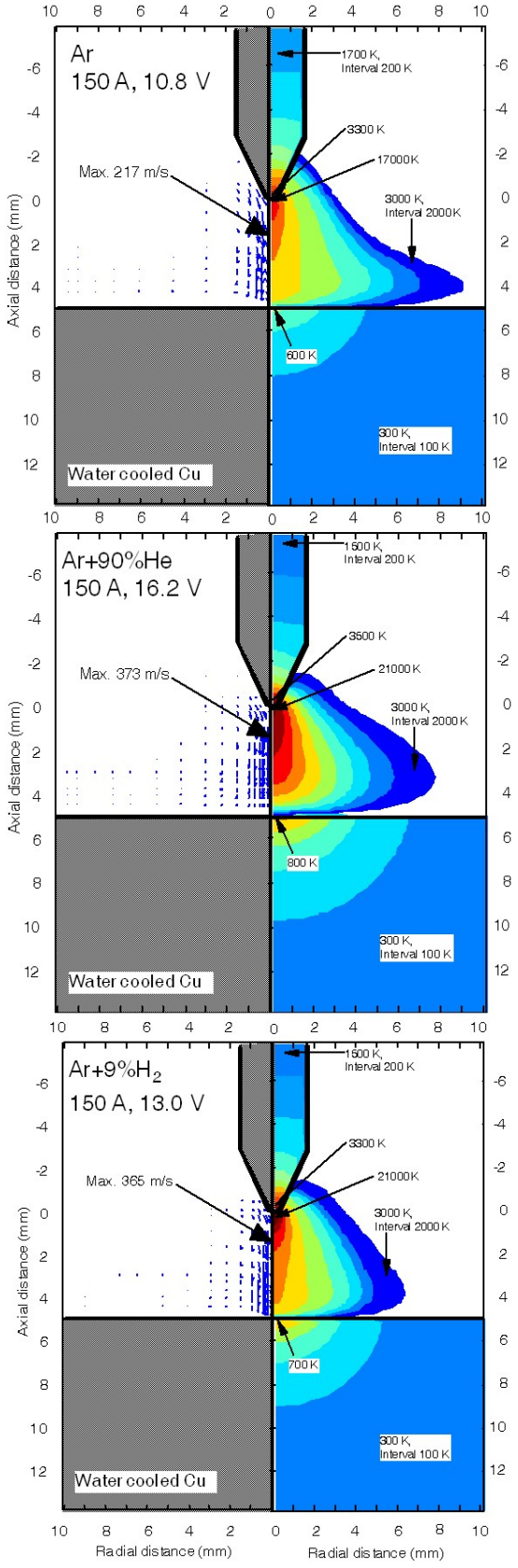

Figure 2: Temperature fields and velocity vectors in the arc and electrodes for 150 A TIG arcs in argon, argon with 90 mol% helium and argon with 9 mol% hydrogen at 1 atm, with a water-cooled copper anode.

Boundary conditions at the top electrode also depend on the polarity. For TIG welding, the top electrode is a doped tungsten cathode, which emits electrons by thermionic emission; boundary conditions are given by Tanaka and Lowke (2007). For MIG welding, the top electrode is a metal wire anode, for which the heat transfer boundary condition is the same as for the workpiece anode in TIG welding, as given in Eq. (8). In MIG welding, the wire anode melts and droplets are transferred to the weld pool; this is not considered in the work described here.

The thermophysical properties of the shielding gases, such as thermal conductivity and electrical conductivity, were taken from Murphy and Arundell (1994) for argon and argon–nitrogen mixtures; Murphy (1997) for argon–helium mixtures, and Murphy (2000) for argon–hydrogen mixtures. Properties for mixtures of iron vapour and argon or helium were calculated using methods similar to those given previously for copper-vapour–argon mixtures (Murphy, 1996). Net radiative emission coefficients were calculated using the method of Cram (1985).

INFLUENCE OF ARC PLASMA ON WELD POOL

As noted above, the values of four arc parameters at the interface with the weld pool are important in determining the influence of the arc plasma on the weld pool: (a) the heat flux, (b) the current density, (c) the shear stress, and (d) the arc pressure.

Increasing the heat flux from the arc to the weld pool increases weld pool depth directly. Equation (8) shows that two factors contribute to the heat flux: electron heating and thermal conduction. The former is typically larger (Tanaka and Lowke, 2007). Since the electron heating term is proportional to the electron current density, which is approximately equal to the total current density, the current density directly affects the weld pool depth via heat transfer. The current density also affects the depth through the magnetic pinch force in Eq. (2), since increased current density increases the downward force on the molten metal, promoting downward flow.

Increased shear stress at the weld pool surface promotes outward flow at the top of the weld pool, and hence upward flow near the weld pool axis. This favours a shallower weld pool. Finally, arc pressure is balanced by the weld pool surface curvature; increased arc pressure gives a more concave surface, which affects the location of the arc attachment to the workpiece. This can lead to further effects that are beyond the scope of this paper, since we assume a flat weld pool surface for simplicity.

EFFECT OF SHIELDING GAS COMPOSITION

We first examine the influence of the shielding gas composition on the arc and weld pool properties for TIG welding. These calculations were performed for a water-cooled copper workpiece, which remains solid. This allows us to focus on the properties of the arc. Figure 2 shows temperatures and velocities for arcs in argon, and mixtures of argon with helium and hydrogen. The addition of helium or hydrogen to the shielding gas increases the maximum arc temperatures and velocities. Only when more than about 30 mol% helium is added are significant changes to arc characteristics observed. In contrast, just 3 mol% hydrogen or 10 mol% nitrogen has a large effect.

Our calculations have shown, in accordance with experiment, that the weld pool shape and depth are strongly dependent on the composition of the shielding gas (Tanaka and Lowke, 2007; Murphy *et al.*, 2009a). For example, Fig. 3 shows the heat flux density to the weld pool is strongly increased by adding helium, hydrogen or nitrogen to argon. The effect of just 3 mol% hydrogen is greater than that of 30 mol% helium, while the effect of 9% helium is greater than that of 90 mol% helium or 20 mol% nitrogen. Figure 3 shows further that there are corresponding increases in the current density.

The shear stress at the workpiece also increases for addition of hydrogen or nitrogen, while adding helium to argon decreases the arc pressure and shear stress, since the high viscosity of helium leads to a lower axial velocity near the axis, as can be seen in Fig. 2. These and similar calculations indicate that the weld pool shape and depth are strongly dependent on the composition of the shielding gas. The addition of hydrogen, nitrogen or helium all leading to increased weld depth, with the effect of increased heat flux and current density dominating the effect of increased shear stress for hydrogen and nitrogen (Tanaka and Lowke, 2007; Murphy *et al.*, 2009a). This implies that the influence of the arc on the weld pool can not be adequately estimated without including the arc in the computational domain.

By modelling TIG arcs in 'imaginary gases', with the thermophysical properties of argon except for one property changed to that of helium, specific heat was found to be the most important thermophysical property in determining the heat flux density and other parameters that influence the weld pool depth (Tanaka *et al.*, 2008, Murphy *et al.*, 2009b). A high specific heat, as is found in mixtures of argon and hydrogen or argon and nitrogen, leads to greater heat flux and current density to the workpiece. In the case of helium, the lower electrical conductivity at temperatures up to about 20 000 K also leads to higher current density and heat flux to the workpiece, as the current is forced to flow through the hotter central regions.

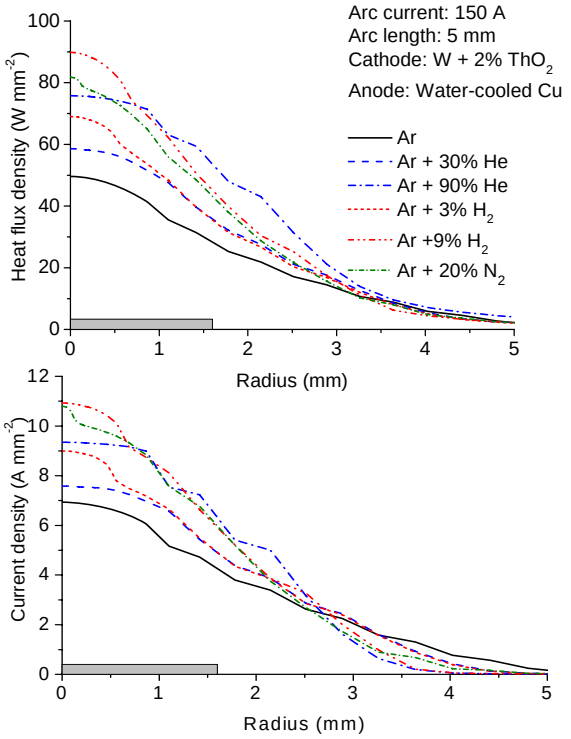

Figure 3: Radial distribution of the heat flux density and current density to the workpiece in TIG welding for mixtures of argon with helium, hydrogen and nitrogen. Percentages are by mole. The radial extent of the cathode is shown by the grey rectangles.

This work has allowed improved shielding gas mixtures (Kimura and Igarashi, 2007) and also new welding processes, such as CO_2-shielded TIG welding (Tanaka *et al.*, 2006) to be developed.

EFFECT OF METAL VAPOUR

The influence of vaporisation of the weld pool metal has been simulated for TIG welding (Yamamoto *et al.*, 2008). The molten weld pool was included self-consistently in the computational domain, although it was assumed its surface remained flat. The metal vapour concentration at the boundary between the arc and the weld pool was calculated using the Clausius–Clapeyron equation. Modelling of the diffusion of the metal vapour required an additional conservation equation, for the mass fraction of metal species (atoms, ions, and electrons derived from the ionisation of metal atoms):

$$\frac{\partial \rho Y_M}{\partial t} + \nabla \cdot (\rho \mathbf{v} Y_M) + \nabla \cdot \mathbf{J}_M = 0 \qquad (10)$$

The diffusion mass flux term was calculated using the 'second viscosity approximation', which is reasonable at the relatively low temperatures near the workpiece (Murphy, 1996).

Figure 4 shows the temperatures, velocities and iron vapour concentrations for a 150 A TIG arcs in helium and argon with a stainless steel workpiece. Vaporisation of elements other than iron was neglected. For the argon arc, the iron vapour concentration reaches a maximum of 0.2 mol%, while for the helium arc, the concentration is much higher, reaching 7.0 mol%. This is because of the higher heat transfer from the helium arc to the weld pool, which leads to a higher weld pool temperature.

As shown in Fig. 5, the heat flux density and current density to the weld pool are strongly decreased by the presence of iron vapour in the helium arc. This is because the presence of the vapour greatly increases the electrical conductivity at temperatures below about 15 000 K, as shown in Fig. 6 This allows current to flow in the cooler regions further from the axis. The influence of iron vapour on the properties of a 150 A argon arc is negligible because of the low concentration of vapour. However, for a higher arc current, the weld pool temperature will be higher and the influence will be larger. The effects for MIG welding are predicted to be even stronger, since in this case vapour is produced from both the wire electrode and the workpiece (Schnick *et al.*, 2009). For both TIG and MIG welding, the influence of the metal vapour means that reliable prediction of weld pool properties requires modelling of the arc.

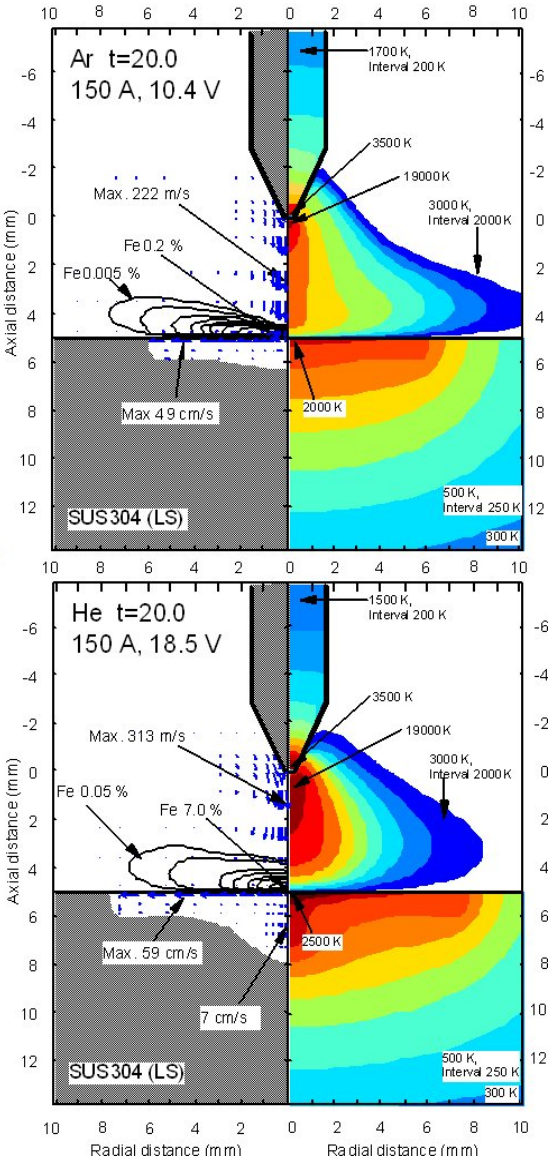

Figure 4: Temperature and iron vapour mass fraction fields and velocity vectors in the arc and electrodes for 150 A TIG arcs in argon and helium at 1 atm with stainless steel workpieces.

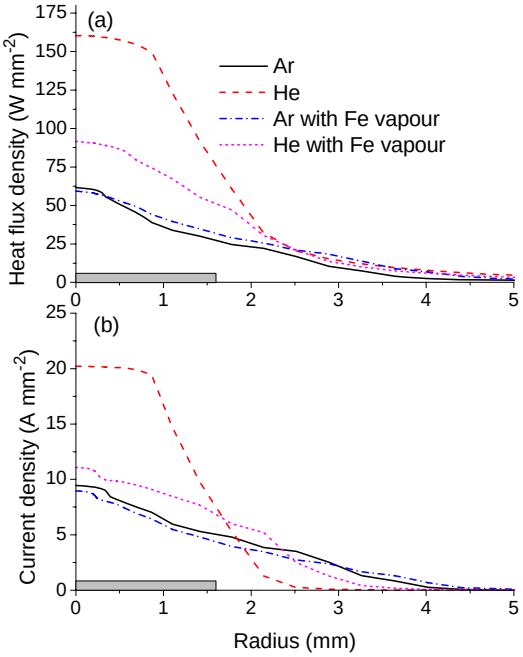

Figure 5: Radial distribution of (a) heat flux density and (b) current density to the workpiece for argon and helium arcs, with and without the influence of iron vapour. The radial extent of the cathode is shown by the grey rectangles.

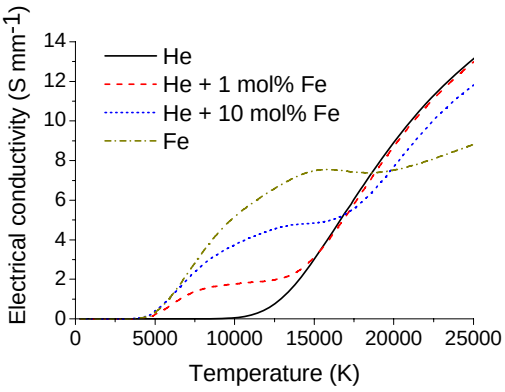

Figure 6: Temperature dependence of the electrical conductivity of helium, iron vapour and mixtures of helium and iron vapour at 1 atm.

EFFECT OF ELECTRODE SHAPE

Changes in electrode shape are particularly large in MIG welding, since the electrode melts and forms droplets. Here we investigate the influence of the electrode shape on the arc properties at the workpiece, by comparing predictions of our model for flat and hemispherical electrode tips. Transfer of metal from the wire electrode to the workpiece and melting of the workpiece were not taken into account for simplicity.

The arc temperature near the electrode was about 10% higher for the hemispherical electrode tip, but the difference in the heat flux density to the workpiece was insignificant. The effect on the convective flow was more substantial; as shown in Fig. 7, the axial velocity is up to about 100 m s^{-1}, or 30%, larger for the hemispherical tip. This is a consequence of the higher magnetic pinch force associated with the higher current density near the tip of the hemispherical electrode.

While the changes to the arc have only a minor effect on the heat flux and current density to the workpiece, the increased axial velocity has a strong influence on the arc pressure and shear stress, as shown in Fig. 8. This in turn will affect the flow in and the shape of the weld pool through the boundary conditions of Eq. (9).

The electrode tip shapes considered here represent only two of a wide range of shapes that occur in MIG welding. Once again, we see that the arc (and in this case the wire electrode) must be included in the computational domain to determine the weld pool geometry reliably.

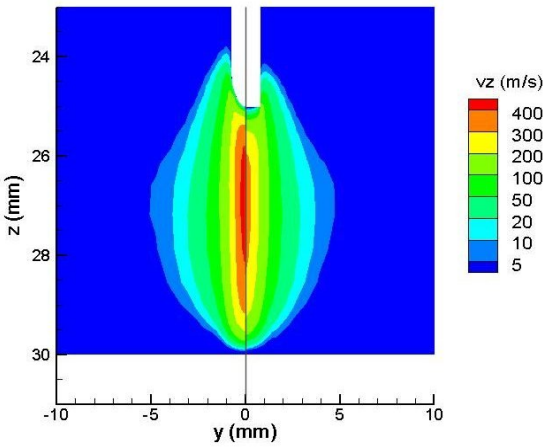

Figure 7: Axial velocity field for 250 A MIG arcs with a hemispherical wire electrode tip (left-hand side) and a flat wire electrode tip (right-hand side). The wire anode and workpiece cathode are shown in white.

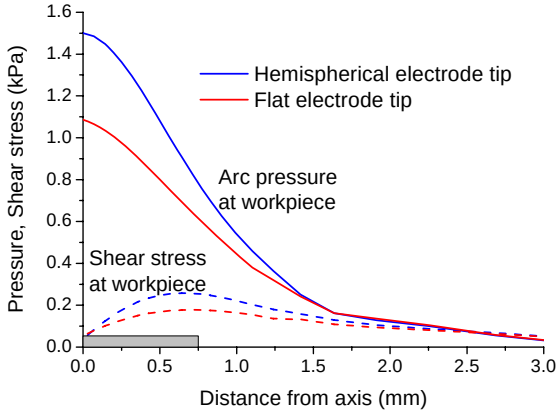

Figure 8: Radial dependence of the arc pressure and shear stress immediately above the workpiece for the MIG arcs shown in Fig. 7. The radial extent of the anode is shown by the grey rectangle.

CONCLUSION

We have shown that the welding gas composition, the production of metal vapour from the weld pool and the electrode shape all strongly influence the properties of the arc and the weld pool. Simulating these phenomena requires the inclusion of the arc plasma in the computational domain, since it is otherwise not possible to determine the required boundary conditions at the interface between the arc and weld pool. Although we have assumed a flat weld pool surface in the examples presented here, if deformation of the surface is considered, then the boundary conditions become more complicated, and necessitate even more strongly the inclusion of the arc plasma in the model.

REFERENCES

CRAM, L.E., (1985), "Statistical evaluation of radiative power losses from thermal plasmas due to spectral lines", *J. Phys. D: Appl. Phys.*, **18**, 401-411.

KIMURA Y. and IGARASHI, Y., Taiyo Nippon Sanso Corporation, (2007), "Welding shield gas and welding method", *US Patent* 7208695-B2.

LOWKE, J.J. and TANAKA, M., (2008), "The physics of non-thermionic cathodes of electric arcs", *Proc. 17th International Conference on Gas Discharges and their Applications*, Cardiff, Wales, September 7-12, pp. 137-140.

MURPHY, A.B. and ARUNDELL, C.J., (1994), "Transport coefficients of argon, nitrogen, oxygen, argon–nitrogen and argon–oxygen plasmas", *Plasma Chem. Plasma Process.*, **14**, 451-490.

MURPHY, A.B., (1996), "A comparison of treatments of diffusion in thermal plasmas", *J. Phys. D: Appl. Phys.*, **29**, 1922-1932.

MURPHY, A.B., (1997), "Transport coefficients of helium and argon–helium plasmas", *IEEE Trans. Plasma Sci.*, **25**, 809-814.

MURPHY, A.B., (2000), "Transport coefficients of hydrogen and argon–hydrogen plasmas", *Plasma Chem. Plasma Process.*, **20**, 279-297.

MURPHY, A.B., TANAKA, M., TASHIRO, S., SATO, T. and LOWKE, J.J., (2009a), "A computational investigation of the effectiveness of different shielding gas mixtures for arc welding", *J. Phys. D: Appl. Phys.*, **42**, 115205.

MURPHY, A.B., TANAKA, M., YAMAMOTO, K., TASHIRO, S., SATO, T. and LOWKE, J.J., (2009b), "Modelling of thermal plasmas for arc welding: the role of shielding gas properties and of metal vapour", *J. Phys. D: Appl. Phys.*, **42**, 194006.

PATANKAR, S.V., (1980), Numerical Fluid Flow and Heat Transfer, Hemisphere, Washington.

SCHNICK, M., FÜSSEL, U., HERTEL, M., SPILLE-KOHOFF, A. and MURPHY, A.B., (2009), "Numerical investigations of diffusion of metal vapour and its influence on arc behaviour in GMA welding", *Proc. 19th International Symposium on Plasma Chemistry*, Bochum, Germany, July 26-31, paper O2-12.

TANAKA, M., TASHIRO, S., USHIO, M., MITA, T., MURPHY, A.B. and LOWKE J.J., (2006), "CO_2-shielded arc as a high-intensity heat source", *Vacuum*, **80**, 1195-1198.

TANAKA, M. and LOWKE J.J., (2007), "Predictions of weld pool profiles using plasma physics", *J. Phys. D: Appl. Phys.*, **40**, R1-R23.

TANAKA, M., TASHIRO, S., SATOH, T., MURPHY, A.B. and LOWKE J. J., (2008), "Influence of shielding gas composition on arc properties in TIG welding", *Sci. Tech. Weld. Join.*, **13**, 225-231.

VAN DOORMAAL, J.P. and RAITHBY G.D., (1984), "Enhancements of the SIMPLE method for predicting incompressible fluid flows", *Numer. Heat Transfer*, **7**, 147-163.

YAMAMOTO, K., TANAKA, M., TASHIRO, S., NAKATA, K., YAMAZAKI, K., YAMAMOTO, E., SUZUKI, K. and MURPHY, A.B., (2008), "Metal vapour behaviour in thermal plasma of gas tungsten arcs during welding", *Sci. Tech. Weld. Join.*, **13**, 566-572.